New Journal of Physics
The open access journal at the forefront of physics

Deutsche Physikalische Gesellschaft DPG
IOP Institute of Physics

Published in partnership with: Deutsche Physikalische Gesellschaft and the Institute of Physics

OPEN ACCESS

RECEIVED
12 March 2015

REVISED
22 June 2015

ACCEPTED FOR PUBLICATION
2 July 2015

PUBLISHED
11 August 2015

PAPER

Coulomb blockade model of permeation and selectivity in biological ion channels

I Kh Kaufman[1], **P V E McClintock**[1,3] **and R S Eisenberg**[2]

[1] Department of Physics, Lancaster University, Lancaster LA1 4YB, UK
[2] Department of Molecular Biophysics and Physiology, Rush Medical College, 1750 West Harrison, Chicago, IL 60612, USA
[3] Author to whom any correspondence should be addressed.

E-mail: i.kaufman@lancaster.ac.uk, p.v.e.mcclintock@lancaster.ac.uk and beisenbe@rush.edu

Keywords: ion channel, Coulomb blockade, electrostatics, nonlinear, stochastic, fluctuational

Abstract

Biological ion channels are protein nanotubes embedded in, and passing through, the bilipid membranes of cells. Physiologically, they are of crucial importance in that they allow ions to pass into and out of cells, fast and efficiently, though in a highly selective way. Here we show that the conduction and selectivity of calcium/sodium ion channels can be described in terms of ionic Coulomb blockade in a simplified electrostatic and Brownian dynamics model of the channel. The Coulomb blockade phenomenon arises from the discreteness of electrical charge, the strong electrostatic interaction, and an electrostatic exclusion principle. The model predicts a periodic pattern of Ca^{2+} conduction versus the fixed charge Q_f at the selectivity filter (conduction bands) with a period equal to the ionic charge. It thus provides provisional explanations of some observed and modelled conduction and valence selectivity phenomena, including the anomalous mole fraction effect and the calcium conduction bands. Ionic Coulomb blockade and resonant conduction are similar to electronic Coulomb blockade and resonant tunnelling in quantum dots. The same considerations may also be applicable to other kinds of channel, as well as to charged artificial nanopores.

1. Introduction

Biological ion channels are natural nanopores providing fast and highly selective permeation of physiologically important ions (e.g. cations such as Na^+, K^+ and Ca^{2+}) through the bilipid membranes of biological cells [1–3]. The channel proteins carrying the pores are embedded in the cellular membrane, and are complicated structures consisting of thousands of atoms.

More than three decades after their discovery, and following a vast number of experiments, a great deal is now known about ion channels. Yet there remain many features of their function—including some quite basic features—that are still not properly understood. Examples include: the *selectivity* in which e.g. a calcium channel favours Ca^{2+} over Na^+ by up to 1000:1, even though the ions are essentially the same size; that this selectivity is combined with *fast permeation* in which the ion goes through the channel almost at the rate of free diffusion (as though the channel were an open hole); the *anomalous mole fraction effect* (AMFE) where, in a pure NaCl solution, a Na^+ ion can pass easily through a calcium channel, but its passage is blocked by tiny traces of Ca^{2+}; the exact role of the *fixed electric charge* at the so-called selectivity filter in determining the selectivity; and, associated with that, the mechanism by which *mutations* that alter the fixed charge can result either in destruction of the channel, so that it no longer conducts, or in conversion of e.g. a sodium channel into a calcium channel or *vice versa*. We will account for these and other experimentally observed features of channel conduction in terms of a novel vision of the permeation process inspired by well-understood phenomena in a quite different area of physics, associated with quantum dots and tunnel diodes.

The conduction and selectivity of a cation-selective channel are determined by the ions' movements and interactions inside a short, narrow selectivity filter lined with negatively charged protein residues that provide the net fixed negative charge Q_f; correspondingly, anion-conducting channels possess positive fixed charge

[1, 4]. Ions in solution are surrounded by hydration shells with associated dehydration potential barriers that are also crucial for selectivity in many cases [5–9]. Selectivity frequently involves a 'knock on' mechanism or, more generally, the correlated motion of several ions [10–13]. The protein residues forming the 'locus' of the selectivity filter are amino acids, of which aspartate (D) and glutamate (E) have negatively charged side chains ($Q_f = -1e$ where e is the proton charge), lysine (K) has a positively charged side chain ($Q_f = +1e$), and alanine (A) has a neutral side chain. The nominal Q_f value is defined by which amino acid residues are present. Calcium L-type channels possess EEEE selectivity filter loci ($Q_f \simeq -4e$) [14–16]. Mammalian Na^+ channels have DEKA inner site loci (and DDEE outer sites) [1, 17] and hence different Q_f. Bacterial NaChBac [18] and NavAb [19, 20] Na^+ channels have selectivity filters with EEEE loci like Ca^{2+} channels *but* select Na^+ ions over Ca^{2+}: an apparent anomaly that awaits explanation.

The modern study of ion channels is based on the existence of the distinct open and closed states of channels, evident in thousands of experiments as discrete levels of current flow measured from individual channel proteins [21]. Site-directed mutagenesis provides a method for systematically varying the structure and net charge of their selectivity filter loci. The resultant changes in conduction and selectivity as functions of Q_f can then be measured by use of the patch-clamp technique. Such mutant studies [18, 22–29] have demonstrated that Q_f is a key determinant of conduction and selectivity in the calcium/sodium family of channels, with the Ca^{2+}/Na^+ selectivity growing with increasing $|Q_f|$ [30–33]. However, the underlying mechanism has remained obscure.

Discovery of the structures of the bacterial potassium KcsA [34] and sodium NavAb [19] channels and the application of all-atom molecular dynamics simulations [20, 28, 35–37] have yielded deep insight into fine details of the ionic permeation processes, including the reproduction of currents [38, 39]. However, a *multi-scale* analysis is still needed [40–42] to build up a full picture. Self-consistent electrostatic and Brownian dynamics simulations [15, 30, 43–45] describe ionic motion as an electro-diffusion process, leading to fast and direct estimation of the currents under non-equilibrium conditions. Such simulations have shown very clearly that the permeation and selectivity features of many channels are defined by just the basic electrostatics of narrow water-filled channels, rather than by the details of the channel structures themselves.

The discreteness of the ionic charge plays a significant role in ion channel conduction [8, 46–48]. An electrostatic theory of ionic transport in water-filled periodically charged nanopores [49, 50], treating the ions as a 1D Coulomb gas [50], revealed ion-exchange through low-barrier phase transitions as the ion concentration and Q_f were varied [51]. It has recently been shown that nanopores can exhibit ionic Coulomb blockade [52], an electrostatic phenomenon similar to electronic Coulomb blockade in mesoscopic systems [53–56].

Our earlier simulations of a simple electrostatic model of calcium/sodium ion channels revealed a periodic set of Ca^{2+} conduction-bands and stop-bands as a function of the fixed charge Q_f at the selectivity filter [57–59] similar to transitions [51]. The energetics of that phenomenon has been derived from electrostatics as single- and multi-ion barrier-less conduction and results were compared with the experimental data available to date [58, 59].

In this paper we demonstrate that the origin of these conduction bands lies in ionic Coulomb blockade [52], closely similar to its electronic counterpart in quantum dots [53]. We thus introduce a Coulomb blockade model of permeation and selectivity in biological ion channels, describing them as discrete electrostatic devices [56]. The applicability of Coulomb blockade to biological ion channels follows naturally from an earlier discussion of the crucial role of electrostatics and the suggestion that there might be 'eigenstates' for conduction [60, 61] in biological ion channels. We will show that the Coulomb blockade model predicts the positions and shapes of the conduction bands, defines the channel occupancy as a Fermi–Dirac distribution, and thereby provides an explanation of divalent block and AMFE, including the exponential dependence of the divalent block threshold IC_{50} on Q_f.

We will focus on the sodium/calcium family of channels including the voltage-gated Ca^{2+} [14, 28] and Na^+ channels [19, 62]. These channels exhibit strong valence selectivity and can undergo a wide range of transformations as the result of site-directed mutagenesis, enabling us to test many of the predictions of our model. The picture that we will develop may, however, be more generally applicable. Section 2 describes a generic model of calcium/sodium channels, its geometry (2.1), electrostatics (2.2), Brownian dynamics (2.3) and validity (2.4). Section 3 introduces and verifies the ionic Coulomb blockade model of ion channel conduction and selectivity; it reviews multi-ion conduction bands (3.1), describes the Coulomb blockade model (3.2), identifies real channels and mutants (3.3), derives the shape of Coulomb blockade oscillations (3.4) and explains the selectivity and AMFE (3.5). Section 3.6 contains further considerations. Section 4 draws the results together and presents concluding remarks.

In what follows, with SI units e is the proton charge, T the temperature, z the ionic valence, k_B Boltzmann's constant and ε_0 the electric permittivity of the vacuum. We use dimensionless units for energy assuming $k_B T = 1$.

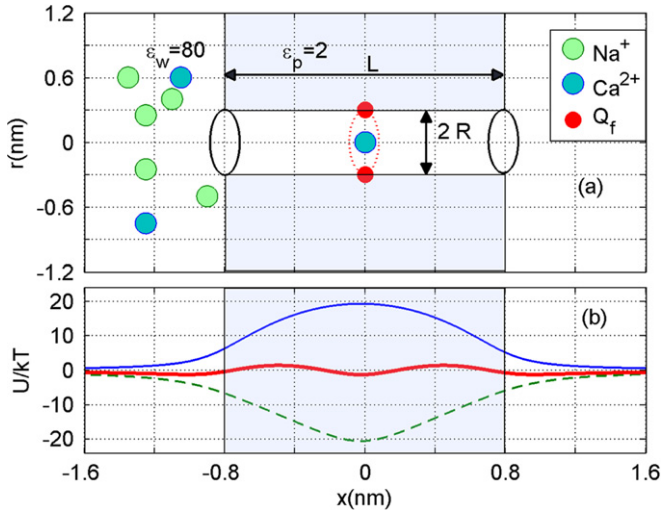

Figure 1. (a) Generic electrostatic model of the selectivity filter of a Ca^{2+} or Na^{+} channel. It is treated as an axisymmetric, water-filled, cylindrical pore of radius $R = 0.3$ nm and length $L = 1.6$ nm through the protein hub in the cellular membrane. A centrally placed, uniform, rigid ring of negative charge Q_f in the range $0 \leqslant |Q_f/e| \leqslant 7$ is embedded in the wall at $R_Q = R$. Ions inside the channel move in single file along its axis. (b) Energetics of a moving Ca^{2+} ion for fixed charge $Q_f = -1e$. The dielectric self-energy barrier U_s (blue solid line) is balanced by site attraction (green dashed line) resulting in an almost barrier-less energy profile (red solid line).

2. A generic electrostatic and Brownian dynamics model of the calcium channel

2.1. Geometry and general features of the model

Figure 1(a) shows the generic, self-consistent, electrostatic model of the selectivity filter of a calcium/sodium channel whose properties we will analyse. We consider it as a negatively charged, axisymmetric, water-filled, cylindrical pore through the protein hub in the cellular membrane; and, to match the dimensions of the selectivity filters of the Na^{+}/Ca^{2+} channels on which we focus, we suppose it to be of radius $R = 0.3$ nm and length $L = 1.6$ nm [14, 15, 63]. The x-axis is coincident with the channel axis, with $x = 0$ in the center of channel. There is a centrally placed, uniformly charged, rigid ring of negative charge $0 \leqslant |Q_f/e| \leqslant 7$ embedded in the wall at $R_Q = R$. The left-hand bath, modeling the extracellular space, contains non-zero concentrations of Ca^{2+} and/or Na^{+} ions. For the Brownian dynamics simulations, the computational domain length $L_d = 10$ nm, its radius $R_d = 10$ nm, the grid size $h = 0.05$ nm, and a potential difference in the range $0 - 25$ mV (corresponding to the depolarized membrane state) was applied between the left and right domain boundaries.

The mobile sodium and calcium ions are described as charged spheres of radius $R_i \approx 0.1$ nm for both ions (allowing use of the implicit solvent model [64, 65] with neglible ion radii), with diffusion coefficients of $D_{\mathrm{Na}} = 1.33 \times 10^{-9}\ \mathrm{m^2\ s^{-1}}$ [15, 66] and $D_{\mathrm{Ca}} = 0.79 \times 10^{-9}\ \mathrm{m^2\ s^{-1}}$ [15], respectively.

We take both the water and the protein to be homogeneous continua describable by relative permittivities $\varepsilon_w = 80$ and $\varepsilon_p = 2$, respectively, together with an implicit model of ion hydration whose validity is discussed elsewhere [58]. We approximate ε_w, D_{Na}, and D_{Ca} as being equal to their bulk values throughout the whole computational domain (see below, section 2.4).

2.2. Self-consistent electrostatics of the model

The electrostatic potential U for an ion, and the potential gradients, were derived by numerical solution of Poisson's electrostatic equation within the computational domain shown in figure 1:

$$-\nabla\left(\varepsilon_0 \varepsilon\, \nabla\phi\right) = \rho_0 + \sum_i e z_i n_i \qquad \text{(Poisson's equation)}, \tag{1}$$

where ε is the relative permittivity of the medium (water or protein), ρ_0 is the density of fixed charge, z_i is the charge number (valence), and n_i is the number density of moving ions.

Self-consistent electrostatics within the narrow, water-filled, channel in the protein differs significantly from bulk electrostatics [49, 67, 68]. The huge gradient between $\varepsilon_w = 80$ and $\varepsilon_p = 2$, the discreteness of ionic charge and the specific channel geometry, lead to permeation, quasi-1D axial behaviour of ions inside the channel [49, 50, 69], and hence to single-filing. Consequently, we use a 1D dynamical model to simulate the axial single-file movement of cations (only) inside the selectivity filter and in its close vicinity.

Figure 1(b) shows axial single-ion potential energy profiles for $Q_f = -1e$, including the repulsive self-energy barrier U_s and the attraction energy U_a attributable to the fixed negative charge. The dielectric self-energy

U_s plays a crucial role in controlling ion permeation through the narrow channel. It will be shown below that U_s defines the strength of Coulomb blockade for an ion of particular valence z, and that it determines the condition for strong valence selectivity [30, 58]. The site attraction is proportional to $z \times Q_f$, so that a variation of Q_f can significantly change the resultant profile. In particular for $Q_f \simeq -1e$, the self-potential barrier of the dielectric boundary force can be balanced by electrostatic attraction to the fixed charge Q_f, resulting in almost barrier-less conduction [58].

2.3. Brownian dynamics simulation of the ionic current

The ions' motion through a channel can be described as an electro-diffusion process and investigated through Brownian dynamics simulations [15, 30, 44, 45, 57, 70–73] of the ionic trajectories. Taking account of the single-filing required by electrostatics, we can solve the over-damped, time-discretized, Langevin equation numerically. An axial step Δx_i of the ith ion is defined as [74],

$$\Delta x_i = -zeD_i \nabla_x \phi(x_i)\Delta t + \sqrt{2D_i \Delta t}\ \xi_i(t) \qquad \text{(Langevin equation)}, \tag{2}$$

where D_i is the ionic diffusion coefficient, Δt is the time step, $\xi_i(t)$ is normalized white noise, z_i is the valence of the ith ion, and the potential $\phi(x_i)$ is calculated self-consistently from (1) at each simulation step.

Brownian dynamics simulations of the ion current J and occupancy P were performed separately for $CaCl_2$ and NaCl solutions, and also for a mixed-salt configuration, with concentrations [Na] = 30 mM and 20 μM $\leqslant$ [Ca] $\leqslant$ 80 mM.

2.4. Validity and limitations of the generic model

Our reduced model obviously represents a considerable simplification of the actual electrostatics and dynamics of moving ions and water molecules within the narrow selectivity filter. The validity and range of applicability of this kind of model have been discussed in detail elsewhere [35, 58, 75, 76]. The most significant simplifications are probably: the use of continuum electrostatics; the use of the implicit solvent model; the use of Brownian dynamics with uncorrelated noise sources for the charged particles; and the assumption of 1D (i.e. single-file) movement of ions inside the selectivity filter. We can partially accommodate these simplifications by use of *effective values* [58].

3. Coulomb blockade model of permeation and selectivity

In this section we introduce the Coulomb blockade picture of permeation and selectivity and show that the phenomenon manifests itself in the model of figure 1 when its geometrical parameters are appropriate for calcium/sodium channels. We will show that the model describes well both the simulated conduction bands and many experimentally measured phenomena of valence selectivity in calcium/sodium channels. The Coulomb blockade model provides significant generalization of our earlier explanation of conduction bands [58] and connects them with mesoscopic transport and single-electron devices [52, 54, 56].

We start by reviewing the main outcome of our earlier Brownian dynamics simulations of conduction bands [57, 58] in order to summarise some of the results that need to be explained including, in particular, the observation of conduction bands.

3.1. Multi-ion conduction bands

Figures 2(a), (b) and 3(a), (b) present the Brownian dynamics results [57–59] for permeation of the model channel figure 1(a) by calcium and sodium ions, respectively, in pure baths of different concentration, plotted in each case as a function of Q_f.

Figure 2(a) exhibits a sequence of narrow conduction bands M_0, M_1, M_2, separated by stop-bands of almost zero-conductance centred on the blockade points Z_1, Z_2, Z_3. Figure 2(b) shows that the M_n peaks in J_{Ca} correspond to transition regimes where the channel occupancy P_{Ca} jumps from one integer value to the next, and that the stop-bands correspond to saturated regions with integer $P_{Ca} = 1, 2, 3$ ....

The band M_0 corresponds to single-ion low-barrier conduction (see red curve in figure 1(b)). Band M_1 corresponds to double-ion knock-on conduction, which is well-established for L-type Ca^{2+} channels [14, 77, 78]; a similar peak was obtained by Corry *et al* [15] in Brownian dynamics simulations of the Ca^{2+} channel. Band M_2 corresponds to triple-ion conduction, a process that can be identified with the permeation of ryanodine receptor calcium channels [7] (see table 1 below for further detail). These bands can be considered as examples of self-organization in ion channels [16, 73].

Comparison of the J_{Ca} and P_{Ca} plots in figures 2(a) and (b) shows that for the M_n points near which conduction occurs, $Q_f = -ze(n + 1/2)$; whereas the non-conducting regions of constant P correspond to Z_n

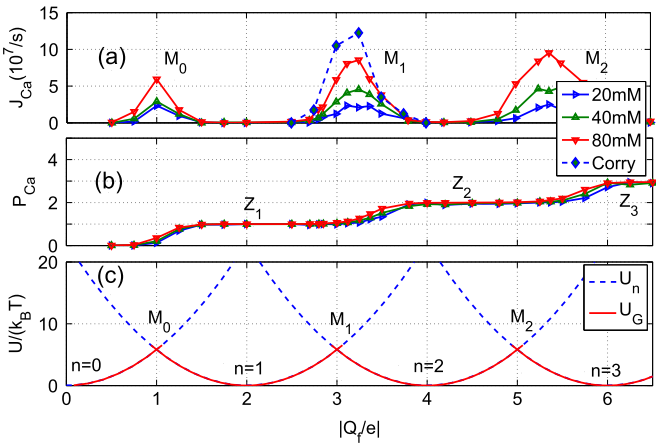

Figure 2. Multi-ion Ca^{2+} conduction and occupancy in the Ca^{2+}/Na^{+} channel model versus the effective fixed charge Q_f; the Brownian dynamics (BD) simulation results (a), (b) are reworked from [57, 59]. (a) Plots of the Ca^{2+} current J_{Ca} for pure Ca^{2+} baths of concentration 20, 40 and 80 mM. The BD results of Corry *et al* [15] are shown for comparison (blue, dashed, diamonds, in arbitrary units). (b) The channel occupancy P_{Ca}. (c) Plots of the electrostatic energy U_n (blue, dashed) and the ground state (i.e. minimum) energy $U_G = \min_n(U_n)$ (red, solid) versus Q_f for channels with $n = 0,\ 1,\ 2,\ 3$. Ca^{2+} ions inside. The conduction bands M_0, M_1, M_2 and the stop bands Z_1, Z_2, Z_3 (indicated by labels) are discussed in the text.

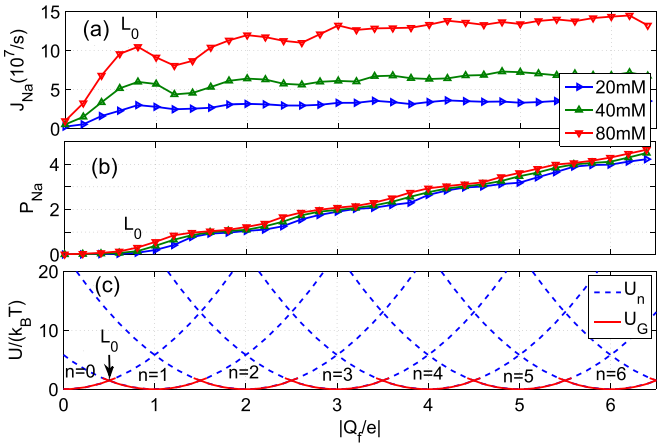

Figure 3. Multi-ion Na^{+} conduction and occupancy in the Ca^{2+}/Na^{+} channel model versus the effective fixed charge Q_f; the Brownian dynamics simulation results (a), (b) are reworked from [59]. (a) Plots of the Na^{+} current J_{Na} for pure Na^{+} baths of concentration 20, 40 and 80 mM. (b) The occupancy P_{Na}. (c) Plots of the electrostatic energy U_n (blue, dashed) and resulting oscillations of the ground state energy $U_G = \min_n(U_n)$ (red, solid) versus Q_f for channels with $n = 0,\ 1,\ 2 \ldots 6$ Na^{+} ions inside. The conduction band L_0 is discussed in the text.

points with $Q_f = -zen$, i.e. to the neutralized state [59]. These bands will be interpreted below as *strong Coulomb blockade*.

Figures 3 (a) and (b) plot the equivalent results for sodium ions in pure NaCl baths of different concentration showing (a) the sodium current and (b) the occupancy as functions of Q_f. The current J_{Na} exhibits a single-ion peak L_0 that would appear to be analogous to the calcium conduction band M_0 of figure 2(a). For larger Q_f there are weak, strongly overlapping, conduction bands between which the current does not fall to zero, making the sodium conductance relatively independent of Q_f. The separations of the J_{Na} band maxima are approximately half the size of those for the calcium bands, reflecting the charge difference between Na^{+} and Ca^{2+} ions. We will refer to this scenario as an example of *weak Coulomb blockade*.

Figures 2(c) and 3(c) plot the ground state energies characteristic of Coulomb blockade graphs [56]. They will be discussed in the next section. Note that we use *ground state* in the physics sense, implying the state of minimum energy.

Table 1. Putative identification of ionic Coulomb blockade model bands with some known wild type (WT) channels and mutants sequences (extended from [58]).

N	Channel/mutant	Site locus	Nom. Q_f/e	Band	Band's Q_f/e
(a)	WT Na^+-selective Nav channel [22]	DEKA	−1	L_0	−0.5
	WT Non-selective OmpF [27]	KRRRDE	−1	M_0	−1
	WT Ca^{2+}-selective *L*-type channel [23]	EEEE	−4	M_1	−3
	WT NaChBac[18], NavAB [28]	EEEE	−4	Z_2	−4
	WT Ca^{2+}-selective RyR channel [7]	DDDD(ED)	−6	M_2	−5
(b)	WT Na^+-selective Nav channel [22]	DEKA	−1	L_0	−0.5
	Ca^{2+}-blocked Nav mutant	⇒ DEKE	−2	M_0	−1
	Ca^{2+}-permeable Nav mutant	⇒ DEEA	−3	Z_1	−2
	Ca^{2+}-selective Nav mutant	⇒ EEEE	−4	M_1	−3
(c)	WT Ca^{2+}-selective *L*-type channel [23]	EEEE	−4	M_1	−3
	Ca^{2+}-blocked Cav mutant	⇒ EEQE	−3	Z_1	−2
	Na^+-conductive Cav mutant	⇒ EEKE	−2	M_0	−1
	Na^+-selective Cav mutant	⇒ EEKA	−1	L_0	−0.5
(d)	WT Na^+-selective NaChBac [18]	EEEE	−4	Z_2	−4
	Ca^{2+}-selective CaChBac mutant	⇒ EEEE+DDDD	−7	M_3	−8
(e)	WT Na^+-selective NavAB [28]	EEEE	−4	Z_2	−4
	Ca^{2+}-selective CavAB mutant	⇒ EEEE+DDDD	−7	M_3	−8

3.2. Coulomb blockade oscillations of conductance

We are now in position to introduce the Coulomb blockade model of conduction and selectivity in Ca^{2+}/Na^+ ion channels. We will find that it is able to account for the pattern of calcium and sodium bands seen in figures 2 and 3 in terms of strong and weak *Coulomb blockade oscillations* [55], respectively .

The discreteness and entity of the ionic charge allow to us to introduce exclusive 'eigenstates' $\{n\}$ of the channel for fixed integer numbers of ions inside its selectivity filter, with total electrostatic energy U_n. The transition $\{n\} \rightarrow \{n+1\}$ corresponds to the entry of a new ion, whereas $\{n\} \rightarrow \{n-1\}$ corresponds to the escape of a trapped ion. The n ions' eigenstates form a discrete exclusive set of $\{n\}$-states [79] :

$$n = \{0,\ 1,\ 2,...\} \qquad \sum_n \theta_n = 1; \qquad P_c = \sum_n n\theta_n, \tag{3}$$

The *electrostatic exclusion principle* (3) leads to Fermi–Dirac statistical distributions [80] for θ_n and P_c, as will be derived below.

The total energy U_n for a channel in state $\{n\}$ can be expressed as:

$$U_n = U_{n,s} + U_{n,a} + U_{n,\mathrm{int}} \tag{4}$$

where $U_{n,s}$ is the self-energy, $U_{n,a}$ is the energy of attraction, and $U_{n,\mathrm{int}}$ is the ions' mutual interaction energy.

We approximate U_n as the dielectric self-energy $U_{n,s}$ of the excess charge Q_n, based on the assumption that both the ions and Q_f are located within the central part of the selectivity filter, so that application of Gauss's theorem to the n similar ions captured within its volume gives a Coulomb blockade-like quadratic dependence of U_n on Q_f [51]:

$$\begin{aligned} U_n &= \frac{Q_n^2 L}{8\pi\varepsilon_0\varepsilon_w R^2} = \frac{Q_n^2}{2C_s} \quad (\text{ Electrostatic energy }) \\ Q_n &= zen + Q_f \qquad\qquad (\text{ Excess charge}). \end{aligned} \tag{5}$$

Here, C_s stands for the geometry-dependent self-capacitance of the channel, and Q_n represents the excess charge at the selectivity filter for the n ions as a function of Q_f. A binomial expansion Q_n^2 in (5) gives first approximations for $U_{n,s}$, $U_{n,a}$ and $U_{n,\mathrm{int}}$ that are consistent with the energetics analysis in [58] and with the 1D Coulomb gas model of ion–ion and ion-fixed charge interactions [49, 50]. A more realistic account of the interactions would result in corrections to (5) and to the formulæ derived from it.

With (5) we arrive at an equation identical to that for electronic Coulomb blockade (except for the presence of z), and our further consideration follows standard Coulomb blockade theory [53, 55]. Remarkably, however, the ionic version of the phenomenon exhibits valence selectivity precisely because it contains the valence z.

To interpret the conduction bands in terms of Coulomb blockade, we calculate U_n as a function of Q_f for $n = 0,\ 1,\ 2,\ 3$ and examine the minimum (i.e. ground state) energy

$$U_G\left(Q_f\right) = \min_n\left(U_n\left(Q_f,\ n\right)\right) \quad (\text{Ground state energy}) \tag{6}$$

for the ground state occupancy n_G, and the excess charge Q_G, all as functions of Q_f (see figures 2(c) and 3(c)). The ground state (6) is by definition a stable state in thermal equilibrium.

Coulomb blockade appears in low-capacitance systems on account of quantization of the quadratic energy in (5) on a grid of discrete states (3), provided that the ground state $\{n_G\}$ is separated from neighbouring $\{n_G \pm 1\}$ states by large Coulomb energy gaps as function of geometry $(R,\ L)$ and ion valence z:

$$U_s = \frac{e^2}{2C_s} = \frac{\lambda_B L}{2R^2}, \quad U_{s,z} = z^2 U_s \gg 1 \quad \text{(Coulomb gap)}, \tag{7}$$

where λ_B stands for Bjerrum length [49] (0.7 nm for water at $T = 298$K). This is the applicability condition for the *strong electrostatic exclusion principle*. Ion channels are extremely small and have tiny capacitance: the dimensionless self-energies of monovalent and divalent ions are $U_{s,1} \approx 5$ and $U_{s,2} \approx 20$, respectively, providing strong Coulomb blockade effects for divalent ions.

It follows from (5) that U_n versus Q_f for given z is described by an equidistant set of identical parabolæ of period equal to the ionic charge ze. These patterns are plotted for Ca^{2+} in figure 2(c) and for Na^+ in figure 3(c). We note that $U_G(Q_f)$ exhibits two different kinds of ground state singular points, marked as M_n and Z_n. The minima of U_n (and correspondingly the blockade regions) appear around the neutralization points $Z_n = -zen$ where the net charge at the selectivity filter $Q_n = 0$ and the occupancy P_c is saturated at an integer value [51, 58].

Figure 2(c) illustrates the fact that for Ca^{2+} the ground state $\{n_G\}$ Z_n points are separated from neighbouring $\{n_G \pm 1\}$ states by an impermeable Coulomb gap of ~20 (see (7)) hence providing strong Coulomb blockade. At the neutralized ($Q_n = 0$) blockade points Z_n, Ca^{2+} ions are prohibited by the self-energy barrier from entering the uncharged channel. The crossover points M_n ($U_n = U_{n+1}$) allow low-barrier (almost barrier-less) $\{n\} \leftrightarrows \{n+1\}$ transitions (see figure 1 (b)); they correspond to the P_c transition regions and to the conduction peaks in J [58]. The M_n points are separated from higher energy states by impermeable barriers of ~40; these points are equivalent to the ion-exchange transitions reported by Zhang *et al* [51].

The pattern of sodium ground states in figure 3(c) arises from energy gaps U_c that are 4× smaller than for calcium, They are too small to prevent thermally activated transitions between neighbouring states and they allow the coexistence of more then two $\{n\}$-states; correspondingly there is only a weak exclusion principle, in turn giving rise to weak Coulomb blockade.

The positions of the singular Q_f points in figure 2(a) can be written as:

$$\begin{aligned} Z_n &= -zen \pm \delta Z_n, && \text{(Coulomb blockade)}, \\ M_n &= -ze\,(n + 1/2) \pm \delta M_n && \text{(Resonant conduction)}, \end{aligned} \tag{8}$$

where δZ_n, δM_n are possible corrections for the singular parts of the affinity and ion–ion interaction (see above) and possible electrostatic field leakage. Equations (8) describe two interleaved periodic sets of points having periods equal to the ionic charge ze, very similar to their counterparts in electronic Coulomb blockade [54].

The points $Z_n = -zen$ are neutralization points, where the excess charge $Q_n = 0$ and U_G takes minimal values. Such points are stable and current is prohibited. Charge neutrality is important, but it is not the only factor that influences channel conductance: the term $\pm\delta Z_n$ accounts formally for the other factors (unaccounted parts of ion–ion/ion-ligand interactions and hydration energy, fields leaks etc).

The points $M_n = -ze\,(n + 1/2)$ are where barrier-less conduction occurs, for which $U_n = U_{n+1}$. Similarly, the terms $\pm\delta M_n$ account formally for any unconsidered perturbations.

We may therefore interpret the Brownian dynamics-simulated calcium conduction bands of figure 2(a) as Coulomb blockade conductance oscillations [55] which appear in this case as $|Q_f|$ is being increased, and the corresponding occupancy steps in figure 2(b) as a Coulomb staircase [56]. The deviations in the precise positions of M_n and Z_n can be attributed to field leaks and the model simplifications.

3.3. Identification of bands with real calcium channels

Table 1, showing the putative identifications of the bands/singularities in the Coulomb blockade model with real channels, wild type and mutants in the Ca^{2+}/Na^+ family, has been extended from [57, 58].

Table 1(a) describes shows identifications of conduction bands with wild type channels.

The single-ion Na^+ barrier-less point L_0 can be speculatively identified with the non-selective DEKA sodium channel ($Q_f = -1e$) [1, 17]. The single-ion Ca^{2+} barrier-less point M_0 can be identified with the non-selective OmpF porin ($Q_f = -1e$) [27], or with nonselective Na^+–K channel [81].

Mammalian calcium channels exist in several modifications. Some of them (L-type, T-type) share the same highly conserved four-glutamate (EEEE) locus at the selectivity filter with nominal $Q_f = -4e$ [14]. The permeation properties (sharp selectivity, AMFE, double-ion nature of calcium permeation) of these channels are consistent with the double-ion M_1 Ca^{2+} conduction band [57, 58]. The double-ion knock-on mechanism of conduction and selectivity in the L-type calcium channel has been derived from the experimentally observed

double-affinity of AMFE [14, 78]. The same M_1 peak can be also identified with the Ca^{2+}-selective mutant of the Nav sodium channel ($Q_f = -3e$) [22] and a calcium-selective mutant of OmpF porin ($Q_f = -4e$) [27].

The Ryanodine receptor RyR calcium channel has $Q_f \approx -6e$ and relatively weak selectivity [7]. We connect it with $M_2 \approx -5e$ three-ion conduction point [57, 58].

Bacterial sodium channels, NaChBac [18] and NavAB [28] possess EEEE loci (with nominal $Q_f = -4e$), typical of mammalian calcium channels but nonetheless exhibit Na^+-selective features and divalent blockade. We connect them (speculatively) with the Z_2 Ca^{2+} blockade point for $Q_f = -4e$.

It is evident that the nominal charges of the channel loci exceed the charge of the model bands by nearly $\Delta Q_f = 1e$. For example, at M_1 we have $Q_f = -3e$ from the Coulomb blockade model, whereas the nominal $Q_f = -4e$ for the EEEE loci of L-type calcium channels (and there are corresponding discrepancies at the M_2 and M_3 points). We speculate that these systematic discrepancies may be connected to field leaks, to the distant influence of the positive charges of the other ends of the amino acids buried in the rest of the protein, or to possible protonation of the side chains [82]. Molecular dynamics simulations [28, 35, 38] could be particularly helpful in determining the effective values of Q_f for wild type and mutant channels.

The above identification scheme can thus account for many mutation transformations observed in the Ca^{2+}/Na^+ channels family. The main test and validation of the Coulomb blockade model is the correct prediction that single $\pm 1e$ mutations should lead to sharp changes of calcium conductance from resonance to blockade and vice versa.

Similarly, table 1(b) describes the radical mutation-induced transformation of the Nav sodium channel to a calcium channel, when the DEKA locus has been sequentially changed by point mutations [22].

Table 1(c) shows that the downward mutations of EEEE calcium channels described in [23] lead to a moderate decrease of divalent/monovalent (Ba^{2+}/Na^+) selectivity for EEEE ($-4e$) $\rightarrow$ EQEE ($-3e$) mutation and a sharp, two-order decrease for the EEEE ($-4e$) $\rightarrow$ EKEE ($-2e$) mutation (though see discussion below).

Tables 1(d), (e) show that the upward mutations of the EEEE loci of bacterial sodium channels (EEEE ($-4e$) $\Rightarrow$ EEEE+DDDD ($-8e$) calcium channels described in [18, 28] lead to channel transformation to a calcium-selective mutant CaChBac and CavAB, respectively. Ca^{2+} selective mutants demonstrate selectivities of up to 600$\times$ in favour of Ca^{2+} ions over Na^+, and AMFE. We putatively connect these transformations with the jump $Z_2 \Rightarrow M_3$. Note, that the model predicts rather high numbers of ions inside the channel (between 3 and 4 for M_3) but there is no experimental evidence to support these specific occupancy numbers.

One of the most striking consequences of the Coulomb blockade oscillations is that, for channels having $Q_f \approx M_n$, adding one negative charge should dramatically *decrease* the Ca^{2+} conductance. So far, all mutation chains showed increase of calcium selectivity with growth of negative Q_f which can also, however, be explained by alternative models [32]. On the other hand these experiments are limited to $|Q_f| \leqslant 4e$ where the Coulomb blockade model also predicts an experimental increase of calcium selectivity with growth of $|Q_f|$ in the range $|Q_f| = 0 - 4e$ (see figure 11 of [58]) but predicts a sharp drop in calcium selectivity near the neutralization blockade point Z_2.

We can suppose that the NavAB/NaChBac EEEE locus has an effective $Q_f = Z_2 = -4e$, and hence a $1e$ mutation of the EEEE ring (or a $\pm 1e$ mutation of the neighbouring ring of residues) should lead to increase of S for both directions of mutation. The currently available data (see tables (d), (e)) were obtained for mutation steps of $Q_s = 4e$ and thus cannot resolve the effect of the smaller $1e$ jumps.

These identifications can be seen as an initial verification of the Coulomb blockade model predictions, albeit with some discrepancies. Further investigations are needed to confirm the channel identifications, to understand why the nominal Q_f is systematically slightly smaller than the Q_f values of band maxima in the model, and to establish the reason why mammalian and bacterial channels with EEEE-loci have opposite selectivity properties.

3.4. Shapes of the Coulomb blockade oscillations

We now develop a description of the (interconnected) shapes of the Coulomb blockade oscillations in J, and the Coulomb staircase in P. We consider the case of divalent Ca^{2+} bands arising from strong Coulomb blockade (figure 2).

The equilibrium distribution of P_c in the vicinity of the M_n points (and hence calculation of the shapes of $P_c(U)$ or $P_c(Q_f)$) follows from standard Coulomb blockade theory. As mentioned above, the energy level separation for divalent Ca^{2+} is so large ($\approx$40) that the general set of eigenstates (3) reduces to a simple two-state exclusive set:

$$m = \{n,\ n+1\}; \quad \theta_n + \theta_{n+1} = 1; \quad P_c = n + \theta_{n+1}. \tag{9}$$

The electrostatic exclusion principle (9) plays the same role here as that of the Pauli exclusion principle in quantum mechanics [83–85]; the standard derivation via the partition function, taking account of exclusion

principle (9) leads [86–88] to Fermi–Dirac statistics for θ_{n+1} and an excess (fractional) occupancy $P_c^* = P_c \bmod 1$:

$$P_c^* = \left(1 + \exp\left(U_{n+1} - \mu\right)\right)^{-1} = \left(1 + P_b^{-1}\exp\left(U_c\right)\right)^{-1}, \tag{10}$$

where $\mu = \mu_0 + \ln P_b$ is the chemical potential, P_b is a reference occupancy related to the bulk concentration, and μ_0 is a constant potential assumed here to be $\mu_0 = \langle U\rangle = (U_n + U_{n+1})/2$. Hence:

$$U_c = U_{n+1} - \mu_0 = \left(U_{n+1} - U_n\right)/2. \tag{11}$$

The Fermi–Dirac equation (10) is equivalent to the Langmuir isotherm [86] and to Michaelis–Menten saturation. A similar Fermi function was obtained earlier [51] for the variation of P_c with concentration.

Note that the Fermi–Dirac distribution needed for cases where the exclusion principle is based on volume exclusion, and the ions have unequal diameters, has been investigated by Liu and Eisenberg [85, 89, 90].

It follows from (5) that U_c is a linear function of Q_f:

$$U_c = k_z\frac{\Delta Q_f}{e}, \tag{12}$$

where $\Delta Q_f = Q_f - M_n$ and $k_z = zU_s$. Hence the Fermi–Dirac function (10) also describes the dependence of P^* on Q_f:

$$P_c^* = \left(1 + P_b^{-1}\exp\left(k_z\frac{\Delta Q_f}{e}\right)\right)^{-1}, \tag{13}$$

where for our geometry with $z = 2$ (Ca^{2+} ions) the dimensionless scaling coefficient $k_z \approx 10$. This is the final result for the shape of the Coulomb staircase of occupancy as a function of Q_f. Figure 2(b) shows qualitative agreement of $P(Q_f)$ shapes with (13), including the concentration-dependent shift between curves with different P_b. We will make a more detailed comparison below.

Approximate forms of the current as a function of energy (or fixed charge) can be found via the variance σ of the Fermi–Dirac occupancy P due to thermal fluctuations, as follows from the fluctuation–dissipation theorem and linear response theory [91]. The ability of an energy level to contribute to the current/conductance is then proportional to $\sigma^2 = \mathrm{d}P/\mathrm{d}U_c$ via the Landauer approximation [54, 55]:

$$\frac{J_c}{J_{\max}} \propto \frac{\mathrm{d}P}{\mathrm{d}U_c} = \cosh^{-2}\left(\frac{U_c}{2}\right), \tag{14}$$

where $J_{\max}$ is the barrier-less diffusive current. Taking account of scattering, one reaches the standard Coulomb blockade theory approximation [55, 92]:

$$\frac{J_c}{J_{\max}} = U_c\sinh^{-1}\left(U_c\right) \approx \cosh^{-2}\left(\frac{U_c}{2.5}\right). \tag{15}$$

Alternatively (15) can be derived by the quasi-equilibrium (or nonequilibrium reaction rate [93]) approach with explicit solution of the Nernst–Planck equation (i.e. the Goldman–Hodgkin–Katz (GHK) solution) taking account of the Fermi–Dirac occupancy (10), so (15) can thus be called the Fermi-GHK approximation; a similar result was obtained earlier by Mott [94, 95].

Figure 4 reveals a resonant conductivity as U_c is varied, for both the Landauer (14) and Fermi-GHK (15) approximations: in each case there is a peak coinciding with the maximum in the derivative of P_c, $\mathrm{d}P/\mathrm{d}U_c$. (Note that, from (5), variation of U_c is equivalent to variation of Q_f.) In practical terms, the difference between the two approximations is small: they both represent double-exponential peaks of half-width $U_{1/2} \approx 2.3$. The form of this current is similar to that of the tunneling current in a quantum dot [54]: an even, double-exponential function of U_c, reflecting the symmetry of the escape and relaxation trajectories [96]. Note that even small asymmetries, easy to overlook, can have disquieting effects [97].

For a quantitative comparison of the theory with P_c as obtained from the Brownian dynamics simulations, we calculate the effective (excess) well depth U_c^* as:

$$U_c^* = \ln\frac{1 - P_c^*}{P_c^*} = k_z\frac{\Delta Q_f}{e}. \tag{16}$$

The Fermi–Dirac function (10) predicts that U_c^* should be linear in Q_f, i.e. (16) represents linearising coordinates for the Fermi–Dirac equation (10); the Coulomb blockade model also predicts the geometry-dependent coefficient k_z.

Figure 5(a) shows a sawtooth-like dependence of U_c^* on Q_f, confirming that the P_c^* transitions obey the Fermi–Dirac function (10) of U_c. For M_1, the slope corresponds well with analytic k_z; the discrepancies in slope at M_2 and M_3 are attributable to our neglect of ion–ion interactions.

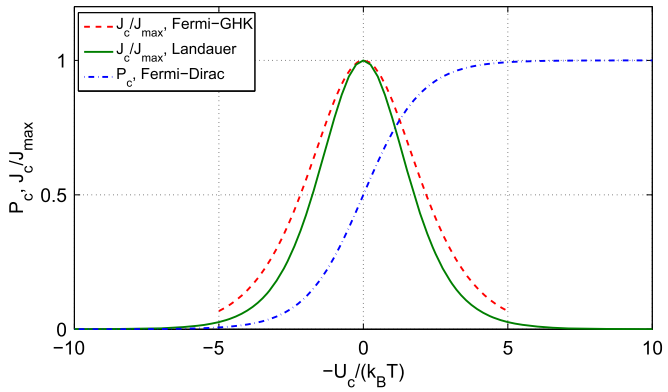

Figure 4. The calculated occupancy P and current J as U_c (or equivalently Q_f) is varied. The occupancy P_c (blue, dash–dot) shows the Fermi–Dirac transition from $P_c = 0$ to $P_c = 1$. The currents calculated in the Landauer $J_c \sim dP/dU$ (green, solid) and Fermi-GHK (red, dashed) approximations both exhibit resonant peaks in the transition region.

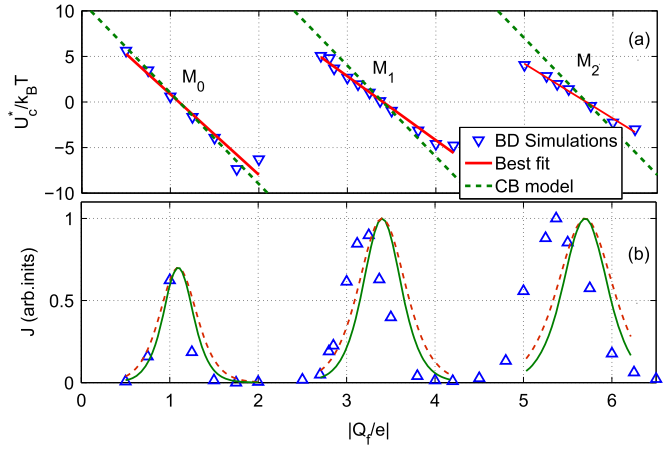

Figure 5. Comparisons of the ionic Coulomb blockade model with Brownian dynamics (BD) simulation results as Q_f is varied. (a) The effective well depth U_c^* (blue point-down triangles) fitted by Fermi–Dirac function (16) with best-fit slopes (full red lines) and with analytical slopes k_z (green dashed lines). (b) The full green curves representing the Landauer approximation (14), and the red-dashed lines representing the Fermi-GHK approximation (15), are compared with the Brownian dynamics simulations (blue, point-up triangles).

Figure 5(b) compares the predictions of the Coulomb blockade model with the conduction bands M_0, M_1, M_2 obtained from the simulations [57]. The Landauer and Fermi-GHK peaks are calculated using (14) and (15) respectively with the values of U_c^* taken from plot (a), and there are no adjustable parameters. The BD peak shapes and positions are described reasonably well by the model, extending the simpler fitting in [58, 59]. Again, the agreement is very good for M_1, and less good for M_2 and M_3 on account of our neglect of field leaks and the singular parts of the interactions.

In general, the results of Brownian dynamics simulations [57, 58] correspond well with the predictions of the Coulomb blockade model.

3.5. Valence selectivity and AMFE

Comparison of the Ca^{2+} ($z = 2$) bands pattern (figure 2) with the Na^+ ($z = 1$) picture (figure 3) clearly shows that, unlike its electronic counterpart, ionic Coulomb blockade is valence-dependent: the positions of the bands $M_0 = ze/2$, and their period ze, shift in proportion to z as described by equation (8) and they broaden/narrow in proportion to z^2 (5) [58].

The ionic Coulomb blockade model attributes selectivity to modification of the U_G dependences on Q_f. Valence selectivity is provided by the electrostatic z-dependent shift of $U_G(n,\ Q_f)$ curves and the corresponding shifts of the M_n and Z_n singular points. Alike-charge selectivity can in principle be accounted for by hydration-dependent shifts of M_n and Z_n.

The model also predicts that a monovalent (e.g. sodium) ionic current can be effectively blocked by a few divalent (e.g. calcium) ions, an effect well-known in calcium and sodium channels. Calcium blockade is an

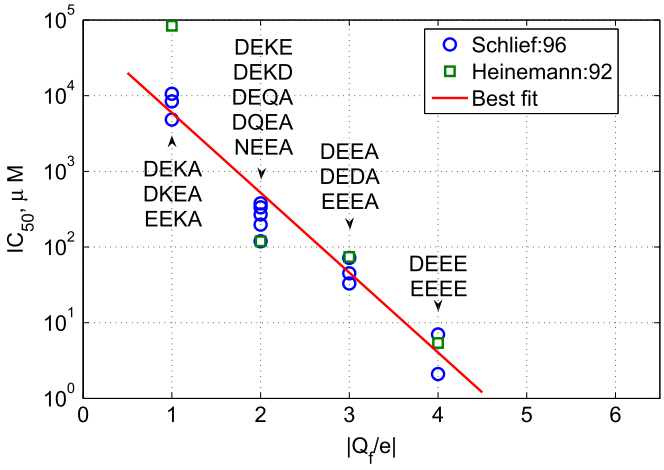

Figure 6. Calcium block as a function of the net charge Q_f of the sodium channel inner ring mutants (relative to the wild type (DEKA)). For the indicated mutants IC_{50} (i.e. the concentration $[Ca^{2+}]$ necessary to block 50% of sodium inward current) is plotted as a function of the net charge of the inner ring Q_f. Data points are taken from [24] (blue open circles) and [22] (green open squares). The continuous red line indicates an exponential function $a\ \exp(-b|Q_f/e|)$, with $b = 2.29$, corresponding to a least-squares fit to all the data.

aspect of AMFE, which is a signature of EEEE calcium channels [14]. The threshold of the divalent block IC_{50} is defined as the Ca^{2+} concentration which results in a 50% decrease in the monovalent current [14]. We can estimate IC_{50} on the assumption that the sodium current is proportional to $(1 - P_{Ca})$, i.e. to the fraction of time when the channel is not blocked by calcium ionc. Hence equations (12, 13) result in an exponential dependence of IC_{50} on Q_f:

$$IC_{50} \propto \exp\left(k_2 \frac{\Delta Q_f}{e}\right), \tag{17}$$

which is a prediction that can be tested.

Mutant studies of the DEKA sodium channel [22, 24, 26] have measured the dependence of AMFE on the selectivity filter locus and its Q_f, and it was shown that $\log(IC_{50})$ can successfully be fitted by a linear function of Q_f (figure 6), in agreement with the prediction (17) of the Coulomb blockade model, or

$$\log\left(IC_{50}\right) = a + b\frac{Q_f}{e}, \tag{18}$$

where a and b are constants. The best-fit line gives $b = 2.29$ [24] which does not agree well with the $b = k_2 \approx 10$ calculated for our model. This discrepancy can be interpreted as evidence that the geometrical parameters (R and L) of the selectivity filter of a DEKA sodium channel differ from values taken in our model ($R = 0.3$ nm, $L = 1.6$ nm). To be compatible with experiments the selectivity filter would need to be shorter and/or wider. We can get good agreement for e.g. $R = 3.5$ nm and $L = 0.4$ nm (such a short selectivity filter would in fact correspond well to the model of [70]) for which $k_2 = 2.28$. Because the exact values are not yet known, our fitting can be used to estimate these parameters. Note, however, that the fitting (18) is not unique to the Coulomb blockade model but follows from the dominance of electrostatics for divalent ions [24].

3.6. Further considerations

Although an ion moving inside a channel is a room-temperature classical system described by Newtonian dynamics, we see that it exhibits some quantum-like mesoscopic features [52]. They include the appearance of strong Coulomb blockade oscillations in conductance, a Coulomb staircase, and a Fermi–Dirac distribution of occupancy for Ca^{2+} ions. We attribute such behavior to the charge discreteness, to the strong electrostatic interaction in confinement [52] and to the electrostatic exclusion principle. It has been shown rigorously that, in the presence of an exclusion principle, Brownian motion leads to a Fermi–Dirac distribution of the Brownian particles [84].

A parametric study [57] based on Brownian dynamics modelling has shown that, in accordance with (7), strong Coulomb blockade may be expected in channels of radii $R = 0.25 - 0.35$ nm for ions having $z = 2$, e.g. for Ca^+ ions in calcium/sodium channels. It is an interesting and significant question whether or not strong blockade and the corresponding oscillations may also arise in the conduction of monovalent ions in K^+ channels. The latter have a selectivity filter of appropriate radius, $R \approx 0.25$ nm [34]. Furthermore, K^+ ions are

fully hydrated, which should lead to a stronger electrostatic interaction and hence to a marked decrease in the effective ϵ_w, bringing it close to $\epsilon_w = 1$. In such a case equation (7) suggests that we could expect an observable Coulomb blockade effect, even for monovalent ions in potassium channels [40, 41], a speculation that needs to be tested.

The relationship of the stop bands in the model to the subconductance states seen in experiments, and to the noise of closed channels, remains to be determined. Subconductance states and unusual baseline noise are found in a wide variety of natural biological channels [98].

4. Conclusions

We conclude that ionic Coulomb blockade manifests itself in a simple electrostatic and Brownian dynamics model of a water-filled charged nanopore with parameters chosen to correspond to those of biological ion channels. It is a fundamental electrostatic phenomenon based on charge discreteness, an electrostatic exclusion principle and linear response theory. For divalent Ca^{2+} ions in calcium/sodium channels, the blockade is strong, so that the ionic permeation process is closely analogous to low-temperature mesoscopic transport in quantum dots. The several similarities include the applicability of Fermi–Dirac statistics and the appearance of Coulomb blockade oscillations, i.e. the calcium ion channel can behave as a single-charge discrete electrostatic device.

For the parameter range where it is applicable and strong, the ionic Coulomb blockade picture leads to several explicit predictions that are unique to the model:

- Periodic oscillations of conductance versus Q_f with a period close to the ionic charge ze, with stop-bands Z_n centred on positions $-zen$, and conduction-bands M_n centred on $-ze\,(n + 1/2)$.
- Hence, a valence dependence of the pattern of bands, leading to valence selectivity.
- Fermi–Dirac occupancy statistics and corresponding shapes of the occupancy bands.
- The barrier-less character of conduction at the M_n points.

The approach also provides straightforward (provisional) explanations of many experimentally observed phenomena in the Ca^{2+}/Na^{+} channels family including:

- Fast permeation, which can be accounted for through barrier-less single- and multi-ion conductivity.
- The strong valence selectivity of calcium channels.
- Divalent block of a monovalent current and the AMFE.
- The mutation transformations of conduction and selectivity.

The ionic Coulomb blockade model of ionic permeation provides a simple and transparent explanation of a wide range of experimental data that hitherto had not seemed to be connected, and it reinterprets the calcium conduction bands as manifestations of a quite general electrostatic phenomenon, common to ion channels, quantum-dots, and tunnel diodes.

Currently available experimental data do not allow for full validation of the Coulomb blockade model and, moreover, there are some small discrepancies. Therefore, we present this theory as something still awaiting full verification through comparison with experimental results from real biological channels, rather than as something already 'verified'. Further investigations are needed to confirm/refute the tentative channel identifications, to understand why the nominal Q_f is systematically slightly smaller than the Q_f values of band maxima in the model, and to explain why mammalian and bacterial EEEE-loci channels have different selectivity properties.

Finally, we remark that the results could also be applicable to other ion channels and to biomimetic nanopores with charged walls.

Acknowledgments

We acknowledge valuable discussions with M I Dykman, W A T Gibby, I A Khovanov, D G Luchinsky, A Stefanovska and R Tindjong. IKK is also grateful to B Shklovskii and M Di Ventra for helpful comments and discussions. The research was supported by the Engineering and Physical Sciences Research Council UK (grants Nos. EP/G070660/1 and EP/M015831/1).

References

[1] Hille B 2001 *Ion Channels Of Excitable Membranes* 3rd edn (Sunderland, MA: Sinauer Associates)
[2] Ashcroft F M 2006 From molecule to malady *Nature* **440** 440–7
[3] Eisenberg B 2013 Ionic interactions are everywhere *Physiology* **28** 28–38
[4] Rubaiy H N and Linsdell P 2015 Location of a permeant anion binding site in the cystic fibrosis transmembrane conductance regulator chloride channel pore *J. Physiol. Sci.* **65** 233–41
[5] Eisenman G and Horn R 1983 Ionic selectivity revisited: the role of kinetic and equilibrium processes in ion permeation through channels *J. Membr. Biol.* **76** 197–225
[6] Laio A and Torre V 1999 Physical origin of selectivity in ionic channels of biological membranes *Biophys. J.* **76** 129–48
[7] Gillespie D 2008 Energetics of divalent selectivity in a calcium channel: the ryanodine receptor case study *Biophys. J.* **94** 1169–84
[8] Zwolak M, Lagerqvist J and di Ventra M 2009 Quantized ionic conductance in nanopores *Phys. Rev. Lett.* **103** 128102
[9] Krauss D, Eisenberg B and Gillespie D 2011 Selectivity sequences in a model calcium channel: role of electrostatic field strength *Eur. Biophys. J.* **40** 775–82
[10] Eisenberg B and Liu W 2007 Poisson–Nernst–Planck systems for ion channels with permanent charges *SIAM J. Math. Anal.* **38** 1932–66
[11] Abaid N, Eisenberg R S and Liu W 2008 Expansions of *I–V* relations via a Poisson–Nernst–Planck system *SIAM J. Appl. Dyn. Syst.* **7** 1507–26
[12] Ji S and Liu W 2012 Poisson–Nernst–Planck systems for ion flow with density functional theory for hard-sphere potential: *I–V* relations and critical potentials: I. Analysis *J. Dyn. Differ. Equ.* **24** 955–83
[13] Liu W, Tu X and Zhang M 2012 Poisson–Nernst–Planck systems for ion flow with density functional theory for hard-sphere potential: *I–V*relations and critical potentials: II. Numerics *J. Dyn. Differ. Equ.* **24** 985–1004
[14] Sather W A and McCleskey E W 2003 Permeation and selectivity in calcium channels *Ann. Rev. Physiol.* **65** 133–59
[15] Corry B, Allen T W, Kuyucak S and Chung S H 2001 Mechanisms of permeation and selectivity in calcium channels *Biophys. J.* **80** 195–214
[16] Giri J, Fonseca J E, Boda D, Henderson D and Eisenberg B 2011 Self-organized models of selectivity in calcium channels *Phys. Biol.* **8** 026004
[17] Catterall W A 2012 Voltage-gated sodium channels at 60: structure, function and pathophysiology *J. Physiol.* **590** 2577–89
[18] Yue L X, Navarro B, Ren D J, Ramos A and Clapham D E 2002 The cation selectivity filter of the bacterial sodium channel, NaChBac *J. Gen. Physiol.* **120** 845–53
[19] Payandeh J, Scheuer T, Zheng N and Catterall W A 2011 The crystal structure of a voltage-gated sodium channel *Nature* **475** 353–8
[20] Corry B 2013 Na^+/Ca^{2+} selectivity in the bacterial voltage-gated sodium channel NavAb *PeerJ* **1** e16
[21] Sakmann B and Neher E (ed) 2009 *Single-Channel Recording* (Berlin: Springer)
[22] Heinemann S H, Teriau H, Stuhmer W, Imoto K and Numa S 1992 Calcium-channel characteristics conferred on the sodium-channel by single mutations *Nature* **356** 441–3
[23] Tang S Q, Mikala G, Bahinski A, Yatani A, Varadi G and Schwartz A 1993 Molecular localization of ion selectivity sites within the pore of a human L-type cardiac calcium channel *J. Biol. Chem.* **268** 13026–9
[24] Schlief T, Schonherr R, Imoto K and Heinemann S H 1996 Pore properties of rat brain 2nd sodium channels mutated in the selectivity filter domain *Eur. Biophys. J.* **25** 75–91
[25] Favre I, Moczydlowski E and Schild L 1996 On the structural basis for ionic selectivity among Na^+ K^+, and Ca^{2+} in the voltage-gated sodium channel *Biophys. J.* **71** 3110–25
[26] Sun Y M, Favre I, Schild L and Moczydlowski E 1997 On the structural basis for size-selective permeation of organic cations through the voltage-gated sodium channel-Effect of alanine mutations at the DEKA locus on selectivity, inhibition by Ca^{2+} and H^+ , and molecular sieving *J. Gen. Physiol.* **110** 693–715
[27] Miedema H, Meter-Arkema A, Wierenga J, Tang J, Eisenberg B, Nonner W, Hektor H, Gillespie D and Meijberg W 2004 Permeation properties of an engineered bacterial OmpF porin containing the EEEE-locus of Ca^{2+} channels *Biophys. J.* **87** 3137–47
[28] Tang L, El-Din T M G, Payandeh J, Martinez G Q, Heard T M, Scheuer T, Zheng N and Catterall W A 2014 Structural basis for Ca^{2+} selectivity of a voltage-gated calcium channel *Nature* **505** 56–61
[29] DeCaen P G, Takahashi Y, Krulwich T A, Ito M and Clapham D E 2014 Ionic selectivity and thermal adaptations within the voltage-gated sodium channel family of alkaliphilic Bacillus *eLife* **3** e04387
[30] Corry B, Vora T and Chung S H 2005 Electrostatic basis of valence selectivity in cationic channels *Biochim. Biophys. Acta—Biomembr.* **1711** 72–86
[31] Boda D, Nonner W, Henderson D, Eisenberg B and Gillespie D 2008 Volume exclusion in calcium selective channels *Biophys. J.* **94** 3486–96
[32] Csányi E, Boda D, Gillespie D and Kristóf T 2012 Current and selectivity in a model sodium channel under physiological conditions: Dynamic Monte Carlo simulations *Biochim. Biophys. Acta—Biomembr.* **1818** 592–600
[33] Dudev T and Lim C 2014 Evolution of eukaryotic ion channels: Principles underlying the conversion of Ca^{2+}-selective to Na^+-selective channels *J. Am. Chem. Soc.* **136** 3553–9
[34] Doyle D A, Cabral J M, Pfuetzner R A, Kuo A, Gulbis J M, Cohen S L, Chait B T and MacKinnon R 1998 The structure of the potassium channel: Molecular basis of K^+ conduction and selectivity *Science* **280** 69–77
[35] Roux B, Allen T, Berneche S and Im W 2004 Theoretical and computational models of biological ion channels *Q. Rev. Biophys.* **37** 15–103
[36] Brooks B R *et al* 2009 CHARMM: The biomolecular simulation program *J. Comput. Chem.* **30** 1545–614
[37] Berneche S and Roux B 2001 Energetics of ion conduction through the K^+ channel *Nature* **414** 73–77
[38] Jensen M Ø, Jogini V, Borhani D W, Leffler A E, Dror R O and Shaw D E 2012 Mechanism of voltage gating in potassium channels *Science* **336** 229–33
[39] Shaw D E *et al* 2008 Anton, a special purpose machine for molecular dynamics simulation *Commun. ACM* **51** 91–7
[40] Kópfer D A, Song C, Gruene T, Sheldrick G M, Zachariae U and de Groot B L 2014 Ion permeation in K^+ channels occurs by direct Coulomb knock-on *Science* **346** 352–5
[41] Hummer G 2014 Potassium ions line up *Science* **346** 303–303
[42] Eisenberg R 2014 Ion channels, natural nanovalves *Encyclopedia of Applied Electrochemistry* ed G Kreysa, K Ota and R F Savinell (Berlin: Springer) pp 1089–93
[43] Hoyles M, Kuyucak S and Chung S-H 1998 Computer simulation of ion conductance in membrane channels *Phys. Rev.* E **58** 3654–61

[44] Im W and Roux B 2002 Ion permeation and selectivity of OmpF porin: a theoretical study based on molecular dynamics, Brownian dynamics, and continuum electrodiffusion theory *J. Mol. Biol.* **322** 851–69
[45] Berti C, Furini S, Gillespie D, Boda D, Eisenberg R S, Sangiorgi E and Fiegna C 2014 Three-dimensional Brownian dynamics simulator for the study of ion permeation through membrane pores *J. Chem. Theory Comput.* **10** 2911–26
[46] Eisenberg B 2002 Proteins, channels and crowded ions *Biophys. Chem.* **100** 507–17
[47] Stopa M 2002 Rectifying behavior in Coulomb blockades: charging rectifiers *Phys. Rev. Lett.* **88** 146802
[48] Millar C, Asenov A and Roy S 2005 Self-consistent particle simulation of ion channels *J. Comput. Theor. Nanosci.* **2** 56–67
[49] Zhang J, Kamenev A and Shklovskii B I 2005 Conductance of ion channels and nanopores with charged walls: a toy model *Phys. Rev. Lett.* **95** 148101
[50] Kamenev A, Zhang J, Larkin A I and Shklovskii B I 2006 Transport in one-dimensional Coulomb gases: from ion channels to nanopores *Physica* A **359** 129–61
[51] Zhang J, Kamenev A and Shklovskii B I 2006 Ion exchange phase transitions in water-filled channels with charged walls *Phys. Rev.* E **73** 051205
[52] Krems M and Di Ventra M 2013 Ionic Coulomb blockade in nanopores *J. Phys.: Condens. Matter* **25** 065101
[53] Averin D V and Likharev K K 1986 Coulomb blockade of single-electron tunneling, and coherent oscillations in small tunnel junctions *J. Low Temp. Phys.* **62** 345–73
[54] Alhassid Y 2000 Statistical theory of quantum dots *Rev. Mod. Phys.* **72** 895–968
[55] Beenakker C W J 1991 Theory of Coulomb-blockade oscillations in the conductance of a quantum dot *Phys. Rev.* B **44** 1646–56
[56] Likharev K K 2003 SET: Coulomb blockade devices *Nano et Micro Tech.* **3** 71–114
[57] Kaufman I K, Luchinsky D G, Tindjong R, McClintock P V E and Eisenberg R S 2013 Multi-ion conduction bands in a simple model of calcium ion channels *Phys. Biol.* **10** 026007
[58] Kaufman I K, Luchinsky D G, Tindjong R, McClintock P V E and Eisenberg R S 2013 Energetics of discrete selectivity bands and mutation-induced transitions in the calcium-sodium ion channels family *Phys. Rev.* E **88** 052712
[59] Kaufman I K, Tindjong R, Luchinsky D G, McClintock P V E and Eisenberg R S 2013 Resonant multi-ion conduction in a simple model of calcium channels *ICNF 2013: Proc. 22nd Int. Conf. on Noise and Fluctuations (Montpellier, 24–28 June)* ed J M Routoure, L Varani and F Pascal pp 1–4
[60] Eisenberg R S 1996 Computing the field in proteins and channels *J. Membr. Biol.* **150** 1–25
[61] Eisenberg R S and Elber R 1996 Atomic biology, electrostatics and ionic channels *New Develop. Theor. Stud. Proteins* **7** 269–357
[62] Catterall W A and Swanson T M 2015 Structural basis for pharmacology of voltage-gated sodium and calcium channels *Mol. Pharmacol.* **88** 141–50
[63] Hu H, Wang Z, Wei R, Fan G, Wang Q, Zhang K and Yin C-C 2015 The molecular architecture of dihydropyrindine receptor/*L*-type Ca^{2+} channel complex *Sci. Rep.* **5** 8370
[64] Boda D, Henderson D and Gillespie D 2013 The role of solvation in the binding selectivity of the *L*-type calcium channel *J. Chem. Phys.* **139** 055103
[65] Fraenkel D 2015 Computing excess functions of electrolyte solutions: The smaller-ion shell model versus the primitive model: II. Ion-size parameters *J. Chem. Theory Comput.* **11** 193–204
[66] Koneshan S, Rasaiah J C, Lynden-Bell R M and Lee S H 1998 Solvent structure, dynamics, and ion mobility in aqueous solutions at 25 C *J. Phys. Chem.* B **102** 4193–204
[67] Parsegian A 1969 Energy of an ion crossing a low dielectric membrane: solutions to four relevant electrostatic problems *Nature* **221** 844–6
[68] Levitt D G 1978 Electrostatic calculations for an ion channel: I. Energy and potential profiles and interactions between ions *Biophys. J.* **22** 209–19
[69] Cheng M H and Coalson R D 2005 An accurate and efficient empirical approach for calculating the dielectric self-energy and ion–ion pair potential in continuum models of biological ion channels *J. Phys. Chem.* B **109** 488–98
[70] Vora T, Corry B and Chung S H 2005 A model of sodium channels *Biochim. Biophys. Acta—Biomembr.* **1668** 106–16
[71] Berti C, Gillespie D, Bardhan J P, Eisenberg R S and Fiegna C 2012 Comparison of three-dimensional Poisson solution methods for particle-based simulation and inhomogeneous dielectrics *Phys. Rev.* E **86** 011912
[72] Tindjong R, Kaufman I, Luchinsky D G, McClintock P V E, Khovanov I and Eisenberg R S 2013 Non-equilibrium stochastic dynamics of open ion channels *Nonlinear Phenom. Complex Syst.* **16** 146–61
[73] Tindjong R, Kaufman I K, Luchinsky D G, McClintock P V E, Khovanov I and Eisenberg R S 2013 Self-organized enhancement of conductivity in biological ion channels *New J. Phys.* **15** 103005
[74] Yesylevskyy S O and Kharkyanen V N 2005 Barrier-less knock-on conduction in ion channels: peculiarity or general mechanism? *Chem. Phys.* **312** 127–33
[75] Tieleman D P, Biggin P C, Smith G R and Sansom M S P 2001 Simulation approaches to ion channel structure-function relationships *Q. Rev. Biophys.* **34** 473–561
[76] Nelissen K, Misko V R and Peeters F M 2007 Single-file diffusion of interacting particles in a one-dimensional channel *Europhys. Lett.* **80** 56004
[77] Hess P and Tsien R W 1984 Mechanism of ion permeation through calcium channels *Nature* **309** 453–6
[78] Armstrong C M and Neyton J 1991 Ion permeation through calcium channels *Ann. New York Acad. Sci.* **635** 18–25
[79] Nelson P H 2011 A permeation theory for single-file ion channels: one- and two-step models *J. Chem. Phys.* **134** 165102–14
[80] Reichl L E and Prigogine I 1980 *A Modern Course in Statistical Physics* (Austin: University of Texas)
[81] Alam A and Jiang Y 2008 Structural analysis of ion selectivity in the NaK channel *Nat. Struct. Mol. Biol.* **16** 35–41
[82] Furini S, Barbini P and Domene C 2014 Effects of the protonation state of the EEEE motif of a bacterial Na^{+}-channel on conduction and pore structure *Biophys. J.* **106** 2175–83
[83] Dirac P A M 1930 *The Principles of Quantum Mechanics* (Oxford: Oxford University Press)
[84] Kaniadakis G and Quarati P 1993 Kinetic equation for classical particles obeying an exclusion principle *Phys. Rev.* E **48** 4263–70
[85] Liu J-L and Eisenberg R 2013 Correlated ions in a calcium channel model: a Poisson–Fermi theory *J. Phys. Chem.* B **117** 12051–8
[86] Fowler R H 1935 A statistical derivation of Langmuir's adsorption isotherm *Math. Proc. Camb. Phil. Soc.* vol 31 (Cambridge: Cambridge University Press) pp 260–4
[87] Zocchi G 2009 Controlling proteins through molecular springs *Ann. Rev. Biophys.* **38** 75–88
[88] Bezanilla F and Villalba-Galea C A 2013 The gating charge should not be estimated by fitting a two-state model to a *Q–V* curve *J. Gen. Physiol.* **142** 575–8
[89] Liu J-L 2013 Numerical methods for the Poisson-Fermi equation in electrolytes, *J. Comput. Phys.* **247** 88–99

[90] Liu J-L and Eisenberg B 2014 Analytical models of calcium binding in a calcium channel *J. Chem. Phys.* **141** 075102
[91] Kubo R 1966 The fluctuation-dissipation theorem *Rep. Prog. Phys.* **29** 255
[92] Kulik I O and Shekhter R I 1975 Kinetic phenomena and charge-discreteness effects in granulated media *Zh. Eksp. Teor. Fiz.* **68** 623–40
[93] Tindjong R, Kaufman I K, McClintock P V E, Luchinsky D G and Eisenberg R S 2012 Nonequilibrium rate theory for conduction in open ion channels *Fluct. Noise Lett.* **11** 1240016
[94] Mott N F and Gurney R W 1957 *Electronic Processes in Ionic Crystals* (Oxford: Clarendon)
[95] Shockley W 1976 The path to the conception of the junction transistor *IEEE Trans. Electron Devices* **23** 597–620
[96] Luchinsky D G and McClintock P V E 1997 Irreversibility of classical fluctuations studied in analogue electrical circuits *Nature* **389** 463–6
[97] Barcilon V, Chen D, Eisenberg R S and Ratner M A 1993 Barrier crossing with concentration boundary conditions in biological channels and chemical reactions *J. Chem. Phys.* **98** 1193–212
[98] Fox J A 1987 Ion channel subconductance states *J. Membr. Biol.* **97** 1–8